

An Eulerian-Based Reduction Model for Iron Ore Particle Reduction

Markus Bösenhofer^{1,2}, Franz Hauzenberger³, Hugo Stocker⁴, Christoph Feilmayr⁵, Michael Harasek¹

¹TU Wien, Institute of Chemical, Environmental and Bioscience Engineering
Getreidemarkt 9/166-2, Vienna, Austria, 1060
Phone: +43-1-58801-166 251
Email: markus.boesenhofer@tuwien.ac.at

²K1-Met GmbH, Area 4 – Simulation and Analyses
Stahlstraße 14, Linz, Austria, 4020

³Primetals Technologies Austria GmbH
Turmstraße 44, Linz, Austria, 4031

⁴voestalpine Stahl Donawitz GmbH
Kerpelystraße 199, Leoben, Austria, 8700

⁵voestalpine Stahl GmbH
voestalpine-Straße 3, Postfach 3, Linz, Austria, 4020

ABSTRACT

Reasonable iron ore reduction and melting prediction are critical issues for blast furnace modeling. The particle number required for full-scale blast furnace simulations exceeds the current capabilities of discrete element method (DEM) approaches. Continuum or Euler-based approaches can handle industry-scale equipment at reduced accuracy. This work explores the capabilities of a novel Eulerian-based reduction model based on a multi-fluid simulation framework. The reduction model uses a layer-like approach based on the representative particle assumption, and its performance is validated and evaluated against lab-scale experimental data.

Keywords: CFD, iron ore reduction, representative particle model (RPM), full-scale blast furnace model

INTRODUCTION

Modeling iron ore reduction is essential for full-scale blast furnace Computational Fluid Dynamics (CFD) models. The reduction process involves various phenomena, e.g., heat and mass transfer, mass transport, and chemistry^{1–3}. In detail modeling can be numerically expensive since a nonlinear, coupled equation system has to be solved for the ore particles. The Lagrangian approach, Euler-Lagrange or CFD-DEM models, is usually employed to model the reduction process due to the discrete nature of the ore particles. Assuming a typical blast furnace size and an average coke and pellet size of 3 cm, some $O(10^8)$ particles are required to model a full-scale furnace. Solving such large systems, including iron ore and coke conversion chemistry, is fiercely numerically expensive and is currently out of reach for Lagrangian approaches.

Continuum models are one way to reduce the numerical effort, but the accuracy of the solid phase flow will be reduced compared to the Lagrangian models. Furthermore, approximating solids by an Eulerian phase neglects detailed particle information and requires unique models for coke and ore thermochemical conversion. Coke conversion can be modeled by a porous particle approach, which assumes isothermal particles and uniform particle size within the computational cells^{4–6}. Unlike coke, iron ore reduction happens in layers with a thin reaction zone separating them⁷. Consequently, a porous approach cannot reasonably predict the reduction process. However, a model for resolving intra-particle heat and mass transport can capture the relevant effects. Since the model is implemented in the continuum approach, a representative particle model (RPM) has to be used⁸. RPMs define a representative particle per computational cell based on local properties.

In this work, we present and validate a numerically efficient RPM for the iron ore reduction within a multi-fluid raceway model^{5,6,9}. The reduction model is developed for the subsequent application in full-scale blast furnace simulations. The following section discusses the model implementation, followed by a model evaluation and validation results.

MODEL DESCRIPTION

1. Modeling Framework

The Eulerian multiphase model used in this work is an add-on for the *multiphaseEulerFoam* solver of the open-source CFD toolbox OpenFOAM®¹⁰. The governing equations of the multiphase model are subsequently presented. The continuity equation per phase is given by:

$$\frac{\partial}{\partial t}(\alpha_i \rho_i) + \nabla \cdot (\alpha_i \rho_i \mathbf{U}_i) = S_{ij} \quad (1)$$

where α_i , ρ_i , and \mathbf{U}_i represent the phase volume fraction, the density, and the velocity vector. S_{ij} is a general mass source term accounting for mass transfer between phases. Due to mass conservation, the sum of S_{ij} over all phases is zero. The species conservation equation of species k per phase is given by

$$\frac{\partial}{\partial t}(\alpha_i \rho_i Y_k) + \nabla \cdot (\alpha_i \rho_i Y_k \mathbf{U}_i) = -\nabla \cdot \alpha_i \mathbf{J}_j + H_{ij,k} + R_k \quad (2)$$

where Y_k , \mathbf{J}_j , $H_{ij,k}$, and R_j are the species mass fraction, the diffusive flux, the inter-phase mass transfer, and the chemistry source term. The energy equation is based on the sensible enthalpy (h_i) and considers compressibility effects, inter-phase heat transfer (Q_{ij}), and the heat release or consumption of the chemical reactions (ΔH_i):

$$\frac{\partial}{\partial t}(\alpha_i \rho_i h_i) + \nabla \cdot (\alpha_i \rho_i h_i \mathbf{U}_i) = \alpha_i \left(\frac{\partial p}{\partial t} + \mathbf{U}_i \cdot \nabla p \right) - \nabla \cdot (\alpha_i \mathbf{q}_i) + \Delta H_i + Q_{ij} \quad (3)$$

p and \mathbf{q}_i are the static pressure and the conductive heat flux. The momentum conservation equation is given by:

$$\frac{\partial}{\partial t}(\alpha_i \rho_i \mathbf{U}_i) + \nabla \cdot (\alpha_i \rho_i \mathbf{U}_i \mathbf{U}_i) = \nabla \cdot \boldsymbol{\sigma}_i + \alpha_i \rho_i \mathbf{g} + \mathbf{K}_{ij} + \mathbf{M}_{ij} \quad (4)$$

It takes into account inter-phase (\mathbf{K}_{ij}) and mass transfer-related (\mathbf{M}_{ij}) momentum exchange rates and gravity (\mathbf{g}). The general Cauchy stress tensor ($\boldsymbol{\sigma}_i$) is used because the stress tensor can differ for fluid and solid phases. Further model details can be found elsewhere^{5,6,9,11}.

2. Iron Ore Reduction Model

A representative particle model (RPM) is used to model the iron ore reduction of an Eulerian solid phase. The RPM creates a fictitious particle based on the solid phase composition, the solid properties, and the particle diameter (d_{RPM}). The particle consists of concentric layers representing a conversion stage and assumes thin reaction zones between two adjacent layers. A leading solid specie represents each conversion stage and tracks the evolution of the layer thickness and other properties, e.g., porosity, tortuosity, and density. Based on experimentally determined iron ore conversion characteristics⁷, these conversion stages are hematite (Fe_2O_3), magnetite (Fe_3O_4), wustite (FeO), and metallic iron (Fe). Figure 1 schematically shows the fictitious particle, including the reaction zones, the external surface, and indicates the diffusive mass transport.

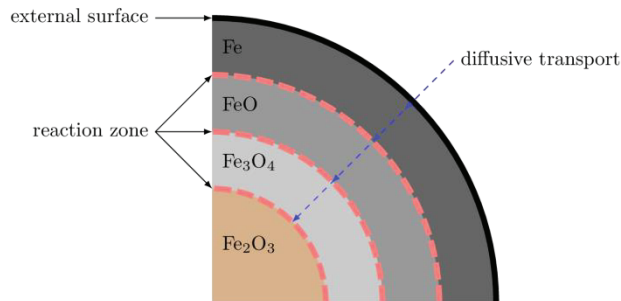


Figure 1: Schematics of the representative particle model.

The equations to calculate the sub-layer volumes (V_i) are calculated using the partial and apparent density and are given by:

$$V_i = V_p Y_{ref,k} \frac{\rho}{\rho_k} \quad (5)$$

where V_p is the particle volume calculated from the particle diameter (d_{RPM}) and $Y_{ref,i}$ and $\rho_{ref,i}$ are the reference specie of the layer and its density.

Typical iron ore reduction models use resistance networks consisting of chemical and diffusive resistances for iron ore reduction^{3,12,13}. Furthermore, these models correct the reducing gas' partial pressure or concentration for the inner reaction layers. This correction increases the numerical effort of the chemistry sub-model. A simplified and more efficient approach is proposed in this work. The two main simplifications are assuming i) an isothermal particle and ii) approximating the partial pressure/concentration correction by additional reaction resistances.

The overall chemical conversion rate ($k_{eq,k-j}$), which can predict ore reduction and oxidation, is given by¹³:

$$k_{eq,k-j} = (k_{eff,k} + k_{eff,j}) \cdot \left(c_k - \frac{c_j}{K_{eq}} \right) \quad (6)$$

where $k_{eff,k}$ and $k_{eff,j}$ are the effective forward (reduction) and reverse (oxidation) rates, while c_k and c_j are the reduction and oxidation gas concentration, and K_{eq} is the equilibrium constant. The effective forward or reverse rate is given by a series circuit similar to¹⁴ which takes into account i) the mass transfer between the gas and particle (first term RHS), ii) the diffusive mass transport to the reactive layer including consumption or production in outer layers (second term RHS), and iii) the chemical conversion rate of the layer (last term RHS):

$$\frac{1}{k_{eff,k}} = \frac{1}{A_s h_{m,k}} + \sum_{l>L} \left(\int_{r_{l+1}}^{r_l} \frac{dA_L}{D_{eff,k} A_L(r)} + \sum \frac{1}{k_{k,L}} \right) + \frac{1}{k_{k,L}} \quad (7)$$

where A_s is the external particle surface, $h_{m,k}$ is the mass transfer coefficient, $D_{eff,k}$ is the pore diffusion coefficient, A_L is the inner layer surface, and $k_{k,L}$ is the chemical rate of the corresponding layer. The Arrhenius equation gives the chemical rate:

$$k_{k,L} = A \cdot \exp\left(\frac{-E_a}{RT_p}\right) \quad (8)$$

where A , E_a , R , and T_p are the rate constant, the activation energy, the ideal gas constant, and the particle temperature. The pore diffusion coefficient is based on the Knudsen ($D_{Kn,i}$) and bulk ($D_{g,i}$) diffusion coefficients and includes a correction for porosity (ε) and tortuosity (τ)^{2,15}:

$$D_{eff,k} = \frac{1}{\left(\frac{1}{D_{Kn,k}} + \frac{1}{D_{g,k}} \right) \tau} \quad (9)$$

The bulk diffusion coefficient is calculated using a simplified Kinetic Gas Theory approach¹⁶ and the Wilke mixing rule. The hematite porosity can be determined experimentally, while the porosities of magnetite, wustite and iron have to be calculated based on the apparent and substance densities:

$$\varepsilon = 1 - \frac{\rho}{\rho_{pure}} \quad (10)$$

The apparent densities of the solids are calculated based on the following relations¹⁷:

$$\rho_{Fe_2O_3} = (1 - \varepsilon_{Fe_2O_3}) \rho_{Fe_2O_3,pure} \quad (11a)$$

$$\rho_{Fe_3O_4} = \rho_{Fe_2O_3} \cdot \frac{|v_{Fe_3O_4}| M_{Fe_3O_4}}{|v_{Fe_2O_3}| M_{Fe_2O_3}} \quad (11b)$$

$$\rho_{FeO} = \rho_{Fe_3O_4} \cdot \frac{|v_{FeO}| M_{FeO}}{|v_{Fe_3O_4}| M_{Fe_3O_4}} \quad (11c)$$

$$\rho_{Fe} = \rho_{FeO} \cdot \frac{|v_{Fe}| M_{Fe}}{|v_{FeO}| M_{FeO}} \quad (11d)$$

The tortuosity is approximated by $\varepsilon^{-0.5}$, which is a reasonable expression for most porous media¹⁸.

The mass transfer coefficient is based on the Sherwood number proposed by¹⁹:

$$h_{m,k} = \frac{Sh_k D_{g,k}}{d_{RPM}} \quad (12)$$

The Gnielinski correlation corrects the mass transfer in the turbulent flow regime:

$$Sh_k = \sqrt{2 + Sh_{lam,k}^2 + Sh_{turb,k}^2} \quad (13)$$

$$Sh_{lam,k} = 0.664 \cdot Re_p^{1/2} Sc_k^{1/3} \quad (14)$$

$$Sh_{turb,k} = \frac{[0.037 \cdot Re_p^{0.8} Sc_k]}{1 + 2.443 \cdot Re_p^{-0.1} (Sc_k^{1/3} - 1)} \quad (15)$$

where $Sh_{lam,k}$, $Sh_{turb,k}$, Re_p , and Sc_k are the laminar and turbulent Sherwood number, the Reynolds number, and the Schmidt number.

The mass consumption/production of a species is given as the sum of the stoichiometric coefficient times the overall rate of all reactions:

$$\frac{dm_k}{dt} = \sum_R k_{eff,R} \nu_{k,R} \quad (16)$$

A coupled system of equations is created from the mass change rates of the involved species and solved for each time step. OpenFOAM® adopts a source linearization approach for chemical source terms. Therefore, the source terms for the species conservation equations are calculated by linearizing the mass change based on the initial and final species mass:

$$H_{ij} = R_k = \frac{m_k(t+\Delta t) - m_k(t)}{\Delta t} \cdot n_p \quad (16)$$

The source term can be interpreted as an interphase mass transfer for the gas phase since the educt is consumed, and the solid phase releases the product. On the contrary, the source term is a chemical for solid species educts and products. The source term has to be corrected by the number of particles inside the computational cell (n_p) since the chemistry is only solved for a single representative particle. The number of representative particles per cell is determined on a volume basis, taking into account the porosity:

$$n_p = \frac{6 \cdot V_{cell} \cdot (1 - \varepsilon)}{d_{RPM}^3 \pi} \quad (18)$$

where V_{cell} is the volume of the computational cell. The previously presented multiphase chemistry model handles species and heat transfer between the gas and solid phase^{5,6,9,11}.

We use a constant iron ore particle diameter in the current implementation since the melting of iron is currently not included. However, a scalar transport equation considering particle shrinkage based on melting rates can be added in the future.

MODEL VALIDATION

The experimental work of Zhang and Ostrovski²⁰ was used to evaluate the proposed RPM for iron ore reduction. A total of five different iron ore reduction experiments are simulated to validate the model implementation. The lab-scale experiment from the literature, the modeling details, and the results will be discussed in the subsequent sub-sections.

1. Validation Experiment

The lab-scale iron ore reduction was performed in a fixed bed reactor inside an electrically heated vertical tube furnace^{20,21}. Figure 2 gives a schematic view of the inner components of the lab-scale reactor. The ore sample is perfused from top to bottom and is kept in place by a ceramic sample holder. Additionally, a thermocouple is positioned at the sample surface to monitor the reduction temperature. The synthetic reduction gas is premixed by a gas mixture station and pre-heated inside the furnace. Further details about the lab-scale reactor can be found elsewhere²¹.

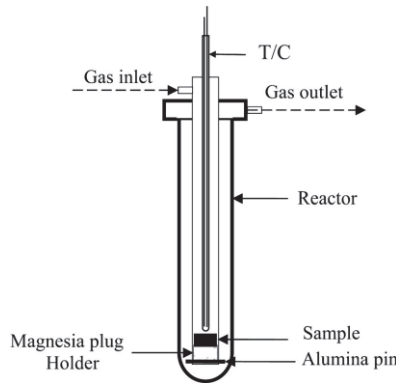


Figure 2: Schematic view of the lab-scale reactor²¹.

Reduction experiments with a 25%_{v/v} H₂ / 75%_{v/v} Ar gas mixture at temperatures of 600 °C, 700 °C, 750 °C, 800 °C, and 925 °C were chosen for the model validation. The experiments used a sample mass of 0.5 g consisting of particles between 0.35 and 0.5 mm and gas flow rates of 1000 mL/min. Reduction degrees (DOR) were determined for various residence times to track the temporal evolution. The DFOR is defined by the molar ratio of O₂ and Fe:

$$DOR = 1 - \frac{n_{O_2}}{1.5 n_{Fe}} \quad (19)$$

The DOE is used for the subsequent evaluation of the simulation model.

2. Simulation Setup

An Eulerian two-fluid approach was used for the iron ore reduction simulations. The Ergun²² and Wakao and Kagueli²³ closures were used for the inter-phase momentum and heat transfer, respectively. As mentioned above, the Gnielinski model¹⁹ determines the mass transfer between the gas and the fictitious particles. Table 1 summarizes the employed reduction reactions and the corresponding kinetic parameters; the CO-based reactions are neglected due to a lack of CO in the reducing agent. The RPM particle size was set to 0.425 mm for the simulations and constant pore size of 200 nm was assumed for the solid particles.

Table 1: Iron ore reduction reactions and kinetic parameters¹³.

Reaction	A (m/s)	E _a (J/mol/K)	K _{eq} (-)
$3Fe_2O_3 + H_2 \leftrightarrow 2Fe_3O_4 + H_2O$	160	92,092	$\exp(-362.6/T + 10.334)$
$Fe_3O_4 + H_2 \leftrightarrow 3FeO + H_2O$	23	71,162	$10^{-3577/T + 3.74}$
$FeO + H_2 \leftrightarrow Fe + H_2O$	15	63,627	$10^{-856.66/T + 0.4387}$

The NASA polynomials and the ideal gas assumption are used for the thermodynamic properties of the gas phase. The iron ore thermodynamics were taken from NIST, except for the heat of formation (h_f), which was determined based on the heat of reaction at 800 °C²⁴. The apparent species density used in the simulations is the porosity-corrected particle density (Eqn. 11). Table 2 summarizes the solid thermodynamic properties.

Table 2: Thermodynamic properties of solid species²⁵.

Specie	c _p (kJ/kg-K)	h _f (kJ/kg)	κ (W/m-K)	ρ (kg/m ³)
<i>Fe</i>	1.063	0	12	1616.8
<i>FeO</i>	0.826	-3280.3	12	2311.6
<i>Fe₃O₄</i>	0.867	-4147.7	12	2537.5
<i>Fe₂O₃</i>	0.943	-4582.4	12	2625.0

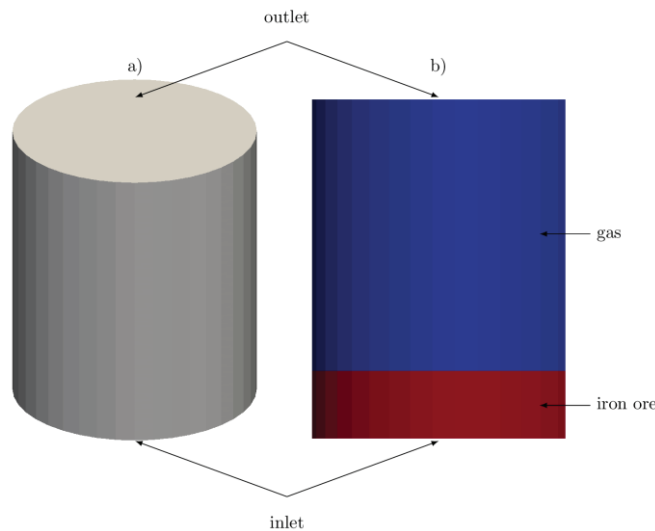


Figure 3: Simplified simulation domain.

The reactor was simplified in the CFD simulations. Only the inner zone, where the iron ore sample is located, is considered. Figure 3 shows the simplified domain, which consists of a simple cylinder. Choosing boundary conditions that correctly represent the physical conditions at the domain's boundaries is tricky. The gas inlet temperature and composition were set according to the reduction temperature and the gas mixture, while zero gradient or Neumann boundary condition was used at the outlet. The pressure boundary conditions are zero gradient at the inlet and a fixed ambient pressure of 1 bar at the outlet. A zero gradient condition is employed at the reactor walls for pressure and species, while a no-slip condition is employed for the

velocity. Contrary, the wall temperature and heat flux are unknown. The two bounding cases are an adiabatic reactor or a perfect heat sink at the wall. Since the actual wall boundary conditions are unknown, we use both cases for the validation.

3. Results

Figure 4 compares the iron or sample's experimental and simulated reduction degrees for the different temperatures. The results indicate that the model predicts a significantly faster reduction for the adiabatic cases. However, the isothermal cases give reduction speeds similar to the experiments. The model fails to predict any ore reduction at a temperature of 600 °C for both cases. The chemical heat release and the consequent temperature increase cause the differences between the adiabatic and isothermal cases. This effect is also visible in the equilibrium reduction degrees; the adiabatic cases predict higher DORs than the corresponding isothermal ones.

The isothermal cases predict slightly faster reduction rates than experimentally measured by Zhang and Ostrovsk²⁰. Two model features can cause this effect: i) employing the educt ambient partial pressure/gas concentration instead of the correct one, or ii) overestimating the mass transport by implicitly assuming educt depletion inside the particle. The effect of assuming isothermality depends on the heat of the reaction. It would slow the conversion down for exothermic reactions and speed the conversion up in case of endothermic reactions. Further investigations are required to quantify the effects of the simplification assumptions. In general, the RPM gives reasonable results for isothermal conditions, despite the simplifications.

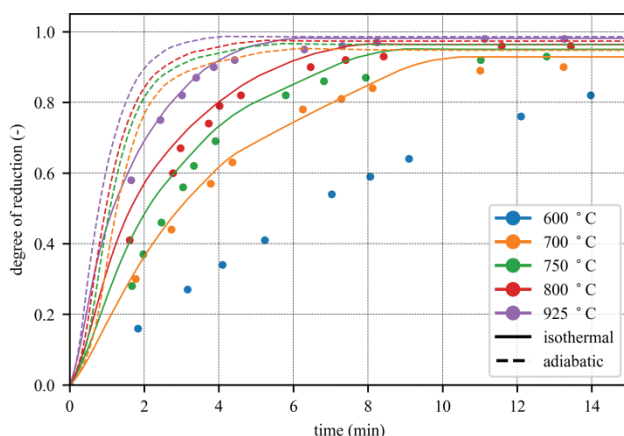


Figure 4: Comparison of mean reduction degree of the experiment and simulation. Experimental data from ²⁰.

CONCLUSIONS

In this work, we presented a simplified, representative particle model (RPM) for iron ore reduction suitable for Eulerian phases. The model creates an isothermal fictitious 1D particle from the Eulerian fields plus a prescribed particle diameter and solves the thermochemical conversion of this particle to obtain species source terms for the Eulerian phase. The implemented model is validated using a lab-scale ore reduction experiment from the literature.

The validation simulations were carried out using two sets of energy boundary conditions: i) adiabatic and ii) isothermal because the actual conditions were unclear from the available data. The simulations indicate that isothermal conditions prevail at the inner reactor walls because the adiabatic cases significantly overestimate the reduction rates. This overestimation is caused by heat accumulation in the reactor. The isothermal reactor simulations reasonably reproduce the experimental data. Furthermore, the equilibrium reduction degrees align with the experimental data, which validates the model implementation and the employed reaction kinetics.

The hematite kinetic reduction rate is low for temperatures around 600 °C but experiences a tenfold rate between 600 °C and 700 °C. A parameter variation revealed that the employed set of physical properties and boundary conditions, in combination with the model simplifications, give a zero rate for 600 °C.

Concluding, the presented simplified and numerically efficient iron ore reduction model proved to reasonably predict iron ore reduction over a wide temperature range. Its reduced numerical effort compared to the DEM or Lagrangian particle models is beneficial for the subsequent use in large- and industrial-scale simulations.

ACKNOWLEDGEMENTS

The authors gratefully acknowledge the funding support of K1-MET GmbH, Metallurgical Competence Center. The research program of the competence center K1-MET is supported by COMET (Competence Center for Excellent Technologies), the

Austrian program for competence centers. COMET is funded by the Federal Ministry for Transport, Innovation and Technology, the Federal Ministry for Digital and Economic Affairs, the province of Upper Austria, Tyrol, and Styria.

Apart from funding, the project activities are financed by the industrial partners Primetals Technologies Austria, voestalpine Stahl and voestalpine Stahl Donawitz.

REFERENCES

1. D. Spreitzer, J. Schenk, Reduction of Iron Oxides with Hydrogen—A Review, *steel research int.* 90 (2019) 1900108.
2. J. Szekely, J.W. Evans, H.Y. Sohn, *Gas-solid reactions*, Academic Press, Cambridge, MA, USA, 1976.
3. Q.T. Tsay, W.H. Ray, J. Szekely, The modeling of hematite reduction with hydrogen plus carbon monoxide mixtures: Part II. The direct reduction process in a shaft furnace arrangement, *AIChE J.* 22 (1976) 1072–1079.
4. M. Harasek, C. Maier, C. Jordan, M. Bösenhofer, C. Feilmayr, in: R.E. Ashburn (Ed.), *AISTech 2016: Proceedings of the Iron & Steel Technology Conference*, 16-19 May 2016, Pittsburgh, Pa. U.S.A, Association for Iron & Steel Technology, Warrendale, Pa., USA, 2016, pp. 353–365.
5. M. Bösenhofer, C. Feilmayr, M. Harasek, F. Hauzenberger, J. Rieger, M. Schatzl, H. Stocker, E. Wartha, in: *AISTech 2021 Proceedings of the Iron and Steel Technology Conference*, AIST, 6/29/2021 - 7/1/2021, pp. 1492–1501.
6. M. Bösenhofer, *On the modeling of multi-phase reactive flows: Thermo-chemical conversion in the raceway zone of blast furnaces*, TU Wien, 2020.
7. E.T. Turkdogan, J.V. Vinters, Gaseous reduction of iron oxides: Part I. Reduction of hematite in hydrogen, *ISIJ International* 2 (1971) 3175–3188.
8. A. Anca-Couce, N. Zobel, H.A. Jakobsen, Multi-scale modeling of fixed-bed thermo-chemical processes of biomass with the representative particle model: Application to pyrolysis, *Fuel* 103 (2013) 773–782.
9. M. Bösenhofer, E. Wartha, C. Jordan, M. Harasek, C. Feilmayr, F. Hauzenberger, B. König, in: *AISTech2019 Proceedings of the Iron and Steel Technology Conference*, AIST, 2019, pp. 2641–2652.
10. H.G. Weller, G. Tabor, H. Jasak, C. Fureby, A tensorial approach to computational continuum mechanics using object-oriented techniques, *Computers in Physics* 12 (1998) 620.
11. M. Bösenhofer, C. Feilmayr, M. Harasek, F. Hauzenberger, H. Stocker, E. Wartha, in: *AISTech 2022 Proceedings of the Iron and Steel Technology Conference*, AIST, 5/16/2022 - 5/18/2022, pp. 198–205.
12. M.E. Kinaci, T. Lichtenegger, S. Schneiderbauer, A CFD-DEM model for the simulation of direct reduction of iron-ore in fluidized beds, *Chemical Engineering Science* 227 (2020) 115858.
13. M.S. Valipour, M.Y. Motamed Hashemi, Y. Saboohi, Mathematical modeling of the reaction in an iron ore pellet using a mixture of hydrogen, water vapor, carbon monoxide and carbon dioxide: an isothermal study.
14. R. Mehrabian, S. Zahirovic, R. Scharler, I. Obernberger, S. Kleditzsch, S. Wirtz, V. Scherer, H. Lu, L.L. Baxter, A CFD model for thermal conversion of thermally thick biomass particles, *Fuel Processing Technology* 95 (2012) 96–108.
15. Charles N. Satterfield, *Mass Transfer in Heterogeneous Catalysis*, The MIT Press, 1969.
16. M. Hishida, A. Hayashi, in: J.-C. Leyer, A.A. Borisov, W.A. Sirignano, A.L. Kuhl (Eds.), *Dynamics of Heterogeneous Combustion and Reacting Systems*, American Institute of Aeronautics and Astronautics, Washington DC, 1993, pp. 343–361.
17. C. Nietrost, *Vereinfachte Modellierung der Eisenpartikel in einem Einschmelzvergaser*, Vienna, 2012.
18. L. Pisani, Simple Expression for the Tortuosity of Porous Media, *Transp Porous Med* 88 (2011) 193–203.
19. V. Gnielinski, Wärme- und Stoffübertragung in Festbetten, *Chemie Ingenieur Technik* 52 (1980) 228–236.
20. J. Zhang, O. Ostrovski, Iron ore reduction/cementation: experimental results and kinetic modelling, *Ironmaking & Steelmaking* 29 (2002) 15–21.
21. J. Zhang, O. Ostrovski, Cementite Formation in CH₄-H₂-Ar Gas Mixture and Cementite Stability, *ISIJ International* 41 (2001) 333–339.
22. S. Ergun, A.A. Orning, Fluid Flow through Randomly Packed Columns and Fluidized Beds, *Ind. Eng. Chem.* 41 (1949) 1179–1184.

23. N. Wakao, S. Kaguci, Heat and mass transfer in packed beds: Topics in chemical engineering 1, Gordon and Breach, 1982, New York, N.Y., 1982.
24. F. Patisson, O. Mirgoux, Hydrogen Ironmaking: How It Works, Metals 10 (2020) 922.
25. P. Linstrom, NIST Chemistry WebBook, NIST Standard Reference Database 69, 1997.